CFD MODELLING OF STARTUP FUELLING PHASE ACCOUNTING FOR ALL HYDROGEN REFUELLING STATION COMPONENTS

Ebne-Abbasi, H.[1], Makarov, D.[2] and Molkov, V.[3]
[1]Hydrogen Safety Engineering and Research Centre (HySAFER) Centre, University of Ulster, Newtownabbey BT37 0QB, UK, ebne_abbasi-h@ulster.ac.uk
[2] dv.makarov@ulster.ac.uk
[3] v.molkov@ulster.ac.uk

ABSTRACT

Further development of hydrogen-fuelled transport and associated infrastructure requires fundamentally based, validated and publicly accepted models for fuelling protocol development, particularly for heavy-duty transport applications where protocols are not available yet. This study aims to use computational fluid dynamics (CFD) for modelling the entire hydrogen refuelling station (HRS) including all its components starting from high-pressure (HP) tanks, a mass flow meter, pressure control valve (PCV), a heat exchanger (HE), nozzle, hose, breakaway and up to 3 separate onboard tanks. The paper focuses on the initial phase of the refuelling procedure, in which the main purpose is to check for leaks in the fuelling line and determine if it is safe to start fuelling. The simulation results are validated against the only publicly available data on hydrogen fuelling by Kuroki and co-authors (2021) from the NREL hydrogen fuelling station experiment. The simulation results – mass flow rate dynamics as well as pressure and temperature at different station locations - show good agreement with the measured experimental data. The development of such models is crucial for the further advancement of hydrogen-fuelled transport and infrastructure, and this study presents a step towards this goal.

1.0 INTRODUCTION

Safety is the highest priority for a wider roll-out of hydrogen technologies including hydrogen fuel cell electric vehicles (FCEV). To persuade the community to migrate to the hydrogen economy, the hazards and associated risks of hydrogen-powered vehicles should be at least at the same level or below those for fossil-fuelled vehicles. Hydrogen, due to its inherently low volumetric energy density, should be compressed for onboard storage to a nominal working pressure (NWP) of 35 MPa for heavy-duty vehicles (HDVs), i.e., buses and trucks, and up to 70 MPa for light-duty vehicles (LDVs), i.e., ordinary cars. During refuelling, hydrogen temperature inside the onboard tanks increases as a result of heat and mass transfer phenomena, including hydrogen compression, the Joule-Thomson effect, the conversion of kinetic energy into internal energy in onboard tanks, etc.

To bear the pressure load of compressed hydrogen, carbon fibre-reinforced polymer (CFRP) is usually used in Type IV tanks. Plus, a hydrogen-tight plastic liner is used to limit permeation to the regulated level [1–3]. Due to the inherent properties of these composite materials, their integrity is endangered when they are exposed to high temperatures while filling tanks to high compression ratios [4]. For this reason, the fuelling protocols mentioned in SAE J2601[5–7], SAE J2579 [1], ISO 15869 [8], European Regulation R134 [3], and UN ECE Regulation GTR#13 [2], limit the allowable temperature inside the tank between -40°C and +85°C, and maximum fuelling pressure by 125% of NWP to prevent the state of charge (SOC) to exceed 100% to ensure the safety of tank while refuelling and its use afterwards. Crossing these limits may jeopardize the safety of the tanks and might even lead to hydrogen tank failure, including rupture, and unignited or ignited (fire) jets caused by hydrogen leaks [9,10]. To stay within the safety allowable temperature range, hydrogen pre-cooling is typically used to keep the final hydrogen temperature in the tank below 85°C [11,12], while it may affect the fuelling station design, performance, reliability and cost [13].

While the SAE J2601 [5] protocol only applies to LDVs with hydrogen capacity up to 10 kg and NWP up to 70 MPa, it is limited to conditions at which the experimental testing was carried out. Besides, it cannot be used to refuel HDVs, i.e., trucks, trains, buses, etc. Unfortunately, SAE J2601-2 [6] and SAE J2601-3 [7] only provide safety guidelines for fuelling HDVs and hydrogen-powered industrial trucks, i.e., forklifts, tractors and pallet jacks, respectively. The underlying physics of heat and mass transfer in

all HRS components and their cumulative effect on the final state of the gasses inside the onboard tank is yet to be fully understood and considered while developing an efficient and cost-effective fuelling protocol. That is why developing and validating contemporary CFD models seems vital.

To reduce the complexity and cost of experimental analysis, computational models are developed to analyze the dynamics of the fuelling process. Reduced models, as a simple and fast tool, are usually focused on filling onboard tanks [14–18]. To the best authors' knowledge, H2Fills [19] is the only reduced model available that is capable of modelling the refuelling process through the entire components of an HRS and is based on the Hydrogen Refuelling Station Dynamic Simulation (HRSDS) software of Kyushu University. There are a couple of limitations for this model including a lack of modelling of HP tank thermal behavior, lack of tank temperature non-uniformity prediction, impossibility to reproduce experimentally observed temperature drop during leak checks, etc. Generally, reduced numerical models are faster and less expensive, but the superior qualities of CFD models could overweight the speed of the reduced models. As an example, reduced models are incapable of modelling temperature non-uniformities inside the onboard tanks. This may lead to a significant increase of localized hydrogen temperature above the calculated by reduced models bulk temperature of 85°C and jeopardize the safety of the composite tanks which may end in its failure during its lifetime usage.

On the other hand, CFD models usually require high computational resources and that's why studies to mention a few [4,12,20–27] were focused on the thermal behaviour of onboard tanks only. In 2018 Bourgeois et al. [28] stressed that it is crucial to take into account the effect of the entire fuelling line while studying the fuelling procedure. In 2021 Kuroki et al. [19] stated that a fuelling model that accounts for the entire fuelling station has not yet been developed and proposed the aforementioned H2Fills reduced model [19]. No CFD model of refuelling through the entire HRS equipment has been reported until this work was carried out at Ulster University during a doctoral study.

The fuelling process is composed of two important sections: startup time and the main fuelling time (Fig. 1). SAE J2601 [5] states that the start-up phase begins after the user initiates fuelling and ends when the dispenser begins flowing hydrogen to fuel the vehicle. This start-up period can include a connection pulse, determination of vehicle tank capacity category, and a leak check [5]. The connection pulse starts when a pressurized nozzle is connected to the receptacle [5]. This specific stage measures any decrease in pressure in the fuelling line [5]. From the safety point of view, the initial connection pulse is vital as it determines if it is safe to start fuelling or not. Failing to pass this check will terminate the fuelling procedure immediately to prevent potential incidents jeopardising life safety and property protection. The start-up phase is an important part of the fuelling protocol aiming to detect possible leaks in the system before proceeding to storage tanks refuelling. This study aims to develop a CFD model for simulations of the refuelling process through the entire set of HRS equipment and compare simulations results against experimental pressure and temperature in onboard tanks during the start-up phase of the refuelling experiment by Kuroki et al. [19] carried out at National Renewable Energy Laboratory (NREL) in the USA.

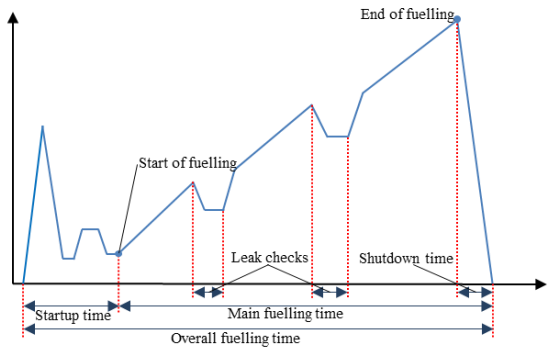

Figure 1. Representation of the start-up time versus overall fuelling time in the SAE J2601 [5].

2.0 EXPERIMENT

The CFD model in this study is validated by the experiment done by Kuroki et al. [19] at the hydrogen refuelling station at the NREL's Hydrogen Infrastructure Testing Research Facility (HITRF). The configuration of this station is similar to actual hydrogen refuelling stations with all the required components including PCV and pre-cooling which both are required for the fuelling procedure recommended by SAE J2601 [19]. Figure 2 shows the components that are used in the experiment [19]. The components include six High-Pressure (HP) tanks with a 300-litre capacity. The HP tanks work in cascade configuration but due to the short duration of the connection pulse, only one of these tanks is used for the start-up phase. The HP tanks are connected through 63 meters of pipes with different cross sections and different wall thicknesses, 24 bends (90-degree), mass flow meter (MFM), HE as the pre-cooler, PCV, breakaway, hose, nozzle and 5 valves to three 36-litres onboard tanks. The onboard tanks have the internal length-to-diameter ratio L/D=3.6 and are placed horizontally. The length, diameter, and material of each piping section, along with the valve flow coefficients are available in the Appendix of the paper [19]. The specification of Piping Section (PS) 9 (pipes from manifolds to onboard tanks) is assumed to be the same for all three pipes based on the H2Fills software demonstration example [19], which replicates the NREL refuelling station and is applied also in this study. All the valves, except the PCV, are assumed to be fully open during refuelling.

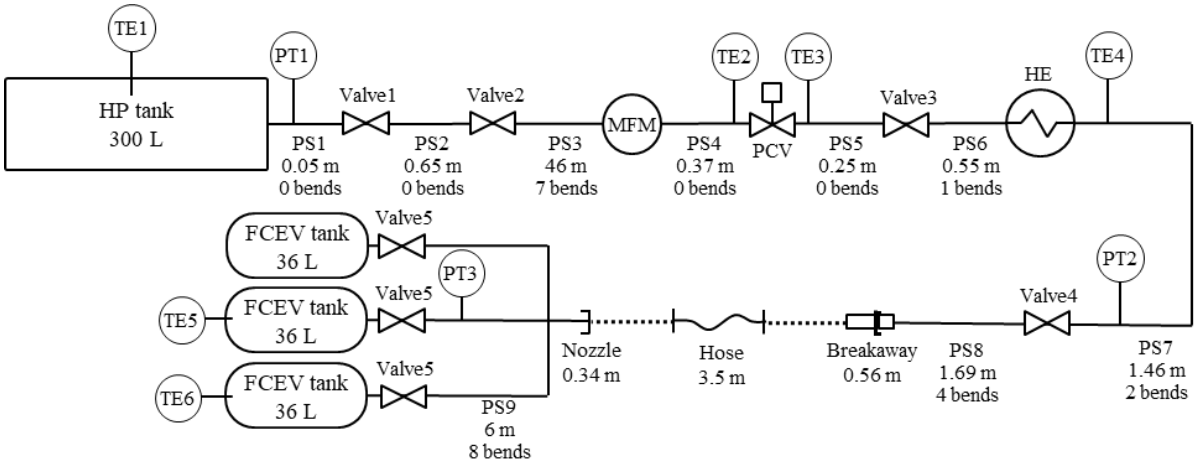

Figure 2. Piping and instrumentation diagram (PID) of the HITRF experimental facility

The experiment was carried out at the ambient temperature of 21°C, HP tank temperature reported as 17.5°C, initial onboard tank pressure 5.5 MPa, initial HP tank pressure 88 MPa, and the Average Pressure Ramp Rate (APRR) of 21.1 MPa/min. The location of pressure transducers (PT) and temperature sensors (TE) are shown in Figure 2. The accuracy of temperature sensors was reported as ±1.5 K and of pressure sensors as ±1.0 MPa [19]. The experimental facility PID also shows temperature sensors (TE5) and (TE6) installed on two of three experimental tanks representing onboard storage. It is worth noting that in the experiment the mass flow rate was not measured directly by an MFM but measured by recording the mass change in the tank. Also, the pressure measured at the tank inlet is assumed to be equal to the gas pressure inside the tank. Two experiments were carried out [19]: Test No.1 with the startup phase but without leak checks during the main fuelling time and Test No.2 with the initial startup phase and two leak checks during the main fuelling time. As the experimental mass flow rate during the startup-up phase of Test No.1 was not recorded and/or reported, Test No.2 was selected for validating the CFD model in this study. Experimentally observed localized temperature drop during leak checks at PCV [19] exit is a subject of our forthcoming study that will be published in due course.

Details of the experimentally measured data for mass flow rate, and pressure and temperature dynamics in the onboard tanks during the start-up phase are presented in the section “Simulation results and discussion” where they are compared against the current study simulation results.

3.0CFD MODEL

3.1 Calculation domain

The calculation domain including all of the HITRF experimental facility components [19] is presented in Fig. 3. It is worth mentioning that the domain boundaries are the internal surfaces of each HRS component. Due to a lack of experimental data for the HP tank in [19], an HP tank with a similar volume and size was designed as a simple cylinder (Fig. 4 a). The length-to-diameter ratio was assumed to be L/D=3 and the thickness of the tank walls, including both CFRP and linear, was estimated as 33 mm. It is worth noting that the onboard tanks are modelled with the same volume, surface area, and L/D as the experimental tanks (Fig 4 b). The computational domain has meshed using 207,252 hexahedral control volumes. The minimum orthogonal quality of the mesh is 0.7 with an average of 0.97.

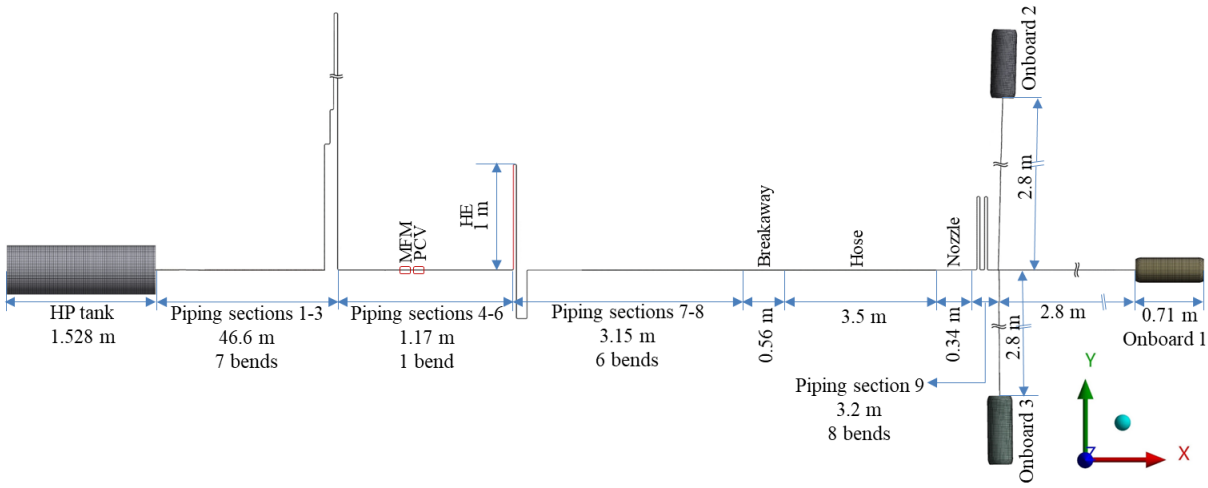

Figure 3. The top view of the computational domain comprises all elements of HRS in the HITRF refuelling experiment.

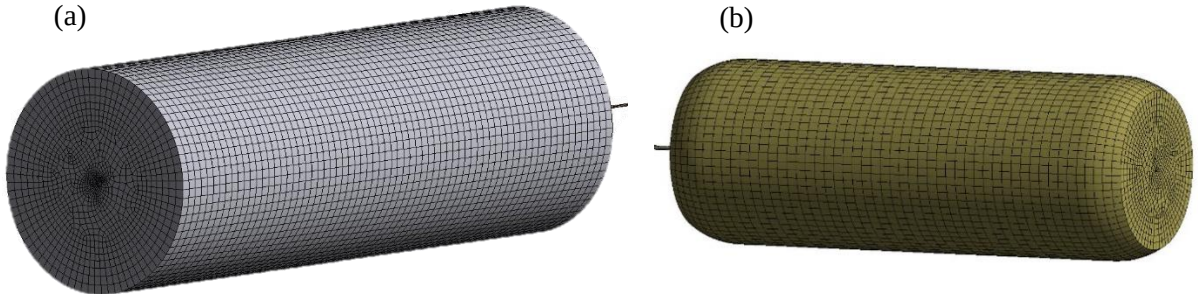

Figure 4. The geometry of the tanks: (a) HP tank and (b) onboard tank (image is not to scale)

Due to the complex geometry of the valves, the valves of this study, including PCV, are modelled as a pipe section. These pipe sections are having an equivalent internal diameter which is calculated based on the experimental valve flow coefficients [19] and they all have a length of 0.1 m. The internal diameter of HE is calculated based on its flow coefficient of 1 [19] and assumed to have a 1 m length to enable us to test different modelling options. The equivalent internal diameters of valves, PCV, MFM and HE is calculated based on the below formula [29]:

$$D_0 = \frac{0.00464986\left(\left(1-\beta^4\right)C_v^2\right)^{\frac{1}{4}}}{\sqrt{C_d}}, \quad (1)$$

in which D_0 is the equivalent pipe diameter, β is the ratio of the equivalent pipe diameter to the upstream pipe size, C_v is the flow coefficient, and C_d is the discharge coefficient.

The values of flow coefficients, C_v were taken from [19] and the discharge coefficient was assumed to be equal to a typical value of C_d=0.65 for valves. The calculated values of the equivalent internal diameter of the PCV, 5 other valves, MFM and HE are shown in Table 1.

Table 1. Calculated equivalent internal diameter of valves, PCV, HE, and MFM using C_v from [19].

Parameter	*Valve1*	*Valve2*	*MFM*	*PCV*	*Valve3*	*HE*	*Valve4*	*Valve5*
Flow coefficient, C_v [28]	1.3	0.75	1.0	1.0	0.75	1.0	0.75	1.0
Calculated equivalent ID [mm]	6.5	4.99	5.76	5.76	4.99	5.76	4.99	5.76

The internal diameter and the length of the pipes are the same as those which are mentioned in [19]. All the bodies between the HP tank and the onboard tanks are treated as cylindrical bodies. The external diameter of the piping sections, breakaway, hose and nozzle was adjusted by Kuroki et al. [19] to match the real weight of these components in order to have the same thermal mass of components as in the experiment. The reported in [19] internal and external diameters along with the properties of a relevant component, i.e. density, specific heat, and thermal conductivity, are used in this numerical study. Because the external diameter and the thermal mass of the valves, PCV, and MFM are not available in [19], it is assumed that these elements have the same external diameter and thermal properties as their upstream pipes.

3.2 Governing equations

Governing equations include unsteady conservation equations for mass, momentum and energy:

$$\frac{\partial \bar{\rho}}{\partial t} + \frac{\partial}{\partial x_j}\left(\bar{\rho}\tilde{u}_j\right) = 0, \tag{2}$$

$$\frac{\partial}{\partial t}\left(\overline{\rho}\tilde{u}_i\right) + \frac{\partial}{\partial x_j}\left(\overline{\rho}\tilde{u}_j\tilde{u}_i\right) = -\frac{\partial \overline{p}}{\partial x_i} + \frac{\partial}{\partial x_j}\left(\mu + \mu_t\right)\left(\frac{\partial \tilde{u}_i}{\partial x_j} + \frac{\partial \tilde{u}_j}{\partial x_i} - \frac{2}{3}\frac{\partial \tilde{u}_k}{\partial x_k}\delta_{ij}\right) + \bar{\rho}g_i, \tag{3}$$

$$\frac{\partial}{\partial t}\left(\bar{\rho}\tilde{E}\right) + \frac{\partial}{\partial x_j}\left(\tilde{u}_j\left(\bar{\rho}\tilde{E} + \overline{p}\right)\right) = \frac{\partial}{\partial x_j}\left(\left(\lambda + \frac{\mu_t c_p}{Pr_t}\right)\frac{\partial \tilde{T}}{\partial x_j}\right). \tag{4}$$

where x_i,x_j,x_k are the Cartesian coordinates, u_i, u_j, u_k are the velocity components, t is the time, p is the pressure, ρ is the density, g_i is the gravity acceleration in i-axis direction, μ and μ_t are the molecular and turbulent dynamic viscosity respectively, δ_{ij} is the Kronecker symbol, E is the total energy, T is the temperature, c_p is the specific heat at constant pressure, λ is the thermal conductivity, Pr_t is the turbulent Prandtl number. The symbol "overbar" stands for Reynolds averaged parameters and "tilde" for Favre averaged parameters.

The model employs the NIST real gas model which uses the National Institute of Standards and Technology (NIST) Thermodynamic and Transport Properties of Refrigerants and Refrigerant Mixtures Database Version 7.0 (REFPROP v7.0) [30], to evaluate the transport and thermodynamic properties of fluids.

Flow turbulence was modelled using the standard k-ε turbulence model [31]:

$$\frac{\partial\left(\overline{\rho}\overline{k}\right)}{\partial t} + \frac{\partial}{\partial x_j}\left(\overline{\rho}\tilde{u}_j\overline{k}\right) = \frac{\partial}{\partial x_j}\left(\left(\mu + \frac{\mu_t}{\sigma_k}\right)\frac{\partial \overline{k}}{\partial x_j}\right) + G_k + G_b - \overline{\rho\varepsilon}, \tag{5}$$

$$\frac{\partial\left(\overline{\rho}\overline{\varepsilon}\right)}{\partial t} + \frac{\partial}{\partial x_j}\left(\overline{\rho}\tilde{u}_j\overline{\varepsilon}\right) = \frac{\partial}{\partial x_j}\left(\left(\mu + \frac{\mu_t}{\sigma_\varepsilon}\right)\frac{\partial \overline{\varepsilon}}{\partial x_j}\right) + C_{1\varepsilon}\frac{\overline{\varepsilon}}{k}\left(G_k + C_{3\varepsilon}G_b\right) - C_{2\varepsilon}\overline{\rho}\frac{\overline{\varepsilon}^2}{k}, \tag{6}$$

where k is the turbulent kinetic energy, ε is the dissipation rate of turbulent kinetic energy, $\mu_t = \bar{\rho} c_\mu \bar{k}^2/\bar{\varepsilon}$, $G_K = \mu_t S^2$, $G_b = -g_i(\mu_t/\bar{\rho}\, Pr_t)(\partial\bar{\rho}/\partial x_i)$, c_m=0.09, σ_k=1.0, σ_e=1.3, $C_{1\varepsilon}$=1.44, $C_{2\varepsilon}$=1.92, $C_{3\varepsilon} = tanh\left|\tilde{u}_y/(\tilde{u}_x^2 + \tilde{u}_z^2)^{0.5}\right|$, $S = \sqrt{2\bar{S}_{ij}\bar{S}_{ij}}$ is the mean rate of strain, $\bar{S}_{ij} = \frac{1}{2}\left(\frac{\partial \bar{u}_i}{\partial x_j} + \frac{\partial \bar{u}_j}{\partial x_i}\right)$.

The simulations were performed using ANSYS Fluent 2020R2 as a CFD engine [32]. The SIMPLE algorithm was applied for pressure-velocity coupling. Convective terms were discretised using the pressure-based implicit solver and first-order upwind numerical scheme. The simulation of 14 s of the start-up phase time takes about 2 hours on a 32-core AMD Opteron CPU running at 2.3 GHz.

3.3 Initial and boundary condition

All the walls in the components are treated as non-slip impermeable walls. The initial temperature and pressure in all the components, including fluids and nearby walls, are the same as in the experiment [19]. The initial pressure in the HP tank and all the pipes between the HP tank and the PCV is 88 MPa, and the pipes from PCV down to the onboard tanks are 5.5 MPa. The initial temperature in the HP tank is 16°C, for the HE is 23°C, and for the rest of the domain is 21°C. Heat flux on all pipe surfaces was calculated using the ANSYS Fluent "shell conduction" capability. The shell conduction calculates conjugate heat transfer through walls in both normal and parallel directions to the pipe axis [32]. After specifying the material properties, e.g. density, specific heat and thermal conductivity, and wall thickness for each section, Fluent automatically grows specified layers of cells, either prismatic or hexahedral, in the wall surface to simulate 3D heat conduction [32]. This model accounts for the specified wall thickness of piping, relevant thermal properties of materials and convective heat transfer on the outer surface of the wall. Fourier's law governs the conduction heat transfer through the walls as follows:

$$\frac{\partial(\rho C_p T)}{\partial t} = \frac{\partial}{\partial x_j}\left(k\frac{\partial T}{\partial x_j}\right), \tag{7}$$

where ρ is density, C_p is specific heat, and k is the thermal conductivity of the wall material. A mixed (3rd) type of boundary condition was set at the external surface of the tank wall:

$$q" = h_{ext}(T_{ext} - T_w), \tag{8}$$

where h_{ext} is the heat transfer coefficient and T_{ext} is ambient temperature; heat transfer coefficient value 7 W/m^2/K is used in line with conclusions in [33].

3.4 Modelling the HE and the PCV

The ANSYS Fluent "fixing the values of variable" option is used to fix the variables in a desired control volume and control temperature in the HE and control the mass flow rate in the PCV. Using this option, the transport equation for a specific variable is not solved in the cell and the cell would not be included when the variable residual sum is computed [32]. A smooth transition between the desired fixed values of the variable and the variables at the neighbouring cell would be the result.

The only detail of the cooling system available in the experimental work [19] is its flow coefficient. Based on that, its equivalent diameter was estimated. The length of the cooling system was assumed to be 1m to expand possible options in the modelling of the HE. Using the User Defined Function (UDF) and the described above "fixing the values of variable" capability of Fluent, the temperature of the fluid passing through the HE zone is set to match the experimentally measured temperature value.

As for the PCV, the mass flow rate is controlled by controlling flow velocity in the PCV. The UDF is programmed to compute the mass flow rate in the PCV ($\dot{m}_{sim}$), compares it with the experimental mass flow rate $\dot{m}_{exp}$, and computes the dimensionless parameter dm_{norm}. This parameter shows the departure of the simulated mass flow rate from the experimental mass flow rate:

$$dm_{norm} = 1 - \frac{\dot{m}_{sim} - \dot{m}_{exp}}{\dot{m}_{exp}}. \quad (9)$$

The velocity of hydrogen in the PCV is changed dynamically based on the value of dm_{norm} to control the required hydrogen mass flow rate in the PCV.

4.0 RESULTS AND DISCUSSIONS

The simulation results of this study were validated using the experimental data from Kuroki et al. [19]. As the experimental raw data was not available, the results from Test No.2 of the experimental study [19] were selected and digitised to be used as the reference for this study.

Figure 5 shows the comparison of the experimental and simulated mass flow rate (right) and temperature after the HE (left) during the start-up phase of 14 s duration. In this study, the mass flow rate of hydrogen and temperature after the pre-cooler were two parameters that were used as input for the model. As these two parameters fed into the model, the pressure and temperature dynamics were simulated in the onboard tanks. It is worth mentioning that the experimental mass flow rate was measured by measuring the mass change in the tanks [19]. However, in the simulation, the mass flow rate was measured in the MFM. As mentioned in the previous section, the model relies on in-house developed UDF which uses the experimental mass flow rate to control velocity in the PCV. Besides, the model controls the temperature in the HE to have similar to the experiment temperature in the TE4 location (after pre-cooler). As can be seen in Fig. 5, the temperature at HE (left) and mass flow rate in the MFM (right) closely follow the experiment with acceptable engineering accuracy.

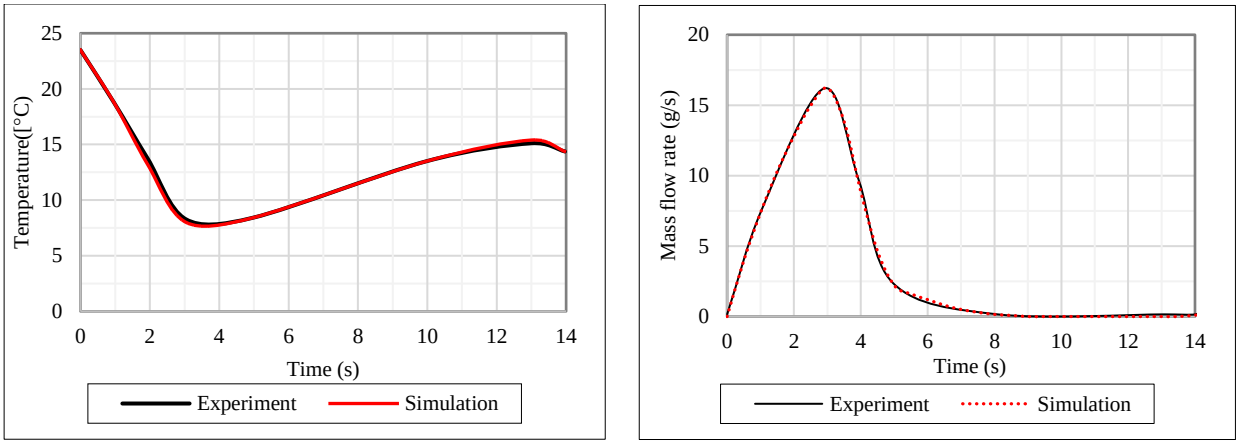

Figure 5. Left: Hydrogen temperature after pre-cooler. Right: Hydrogen mass flow rate at the MFM

The analysis of experimental dynamics in mass flow rate and temperature after the PCV indicates that the heat exchanger (HE) begins functioning when the PCV opens to generate a connection pulse. Furthermore, the cooling of the HE is turned off when the PCV starts closing. This observation suggests that the reason why the temperature at the HE exit stops decreasing and starts to increase after the mass flow rate starts decreasing is due to the functioning of the HE during the opening and closing of the PCV.

The information presented in Fig. 6 depicts the changes in pressure and temperature within the onboard tanks during the initial stage of fuelling. The location of thermocouples used in the experiment was situated in the centre of the onboard tanks. The simulation model adopted the same measuring points for pressure and temperature as used in the experiment. The difference in maximum pressure between the simulation and the experiment is less than 0.1 MPa, which is an outstanding outcome given that the accuracy of pressure transducers with a maximum pressure of over 100 MPa is quite high at approximately 1 MPa [19].

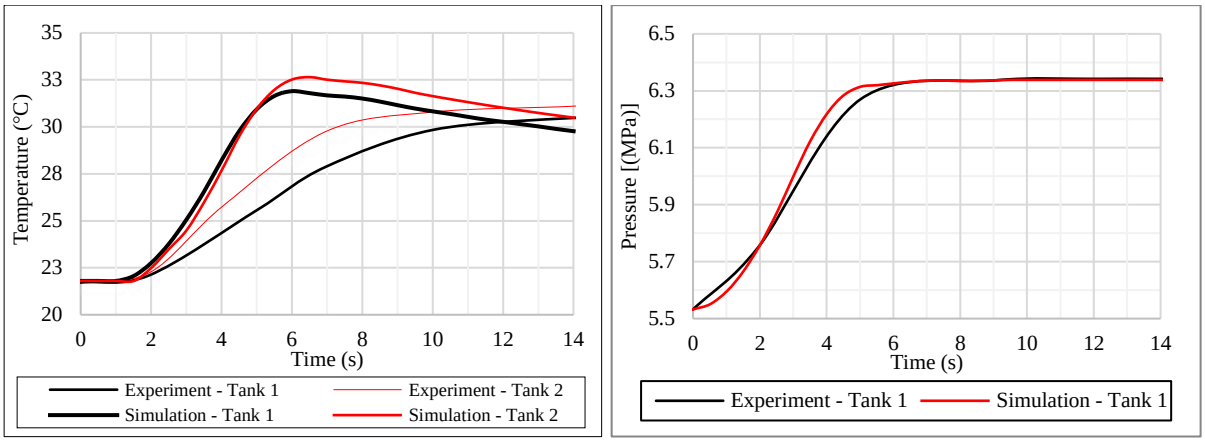

Figure 6. Left: simulated instantaneous temperature in the tank centre versus experimentally measured temperature in the two onboard tanks. Right: simulated versus experimental pressure in the onboard tank 1.

According to the simulations, the temperature at the centre of the onboard tank (shown in Fig. 6, left) reaches its maximum value towards the end of the connection pulse (as indicated by the change in mass flow rate over time, depicted in Fig. 5, right). Subsequently, the temperature decreases due to heat transfer to the cooler tank walls, which is consistent with the findings of other experiments conducted by Kuroki et al. [17] . However, the experimental temperature transients observed during the validation test, as shown in Test No. 2 of Kuroki et al. [19], indicate a continuous increase in temperature until the end of the 14-second start-up period (as depicted in Fig. 6, left). This temperature dynamics in the experiment is somewhat unexpected because hydrogen ingress into the onboard tank (i.e., compression) stops after 8 seconds of the start-up phase. Despite this, the experimental temperature continues to increase even after 8 seconds when the mass flow rate into the tanks is zero, and the pressure transient depicted in Fig. 6 (right) shows that the pressure inside the tanks remains constant after 8 seconds from the beginning of the start-up phase.

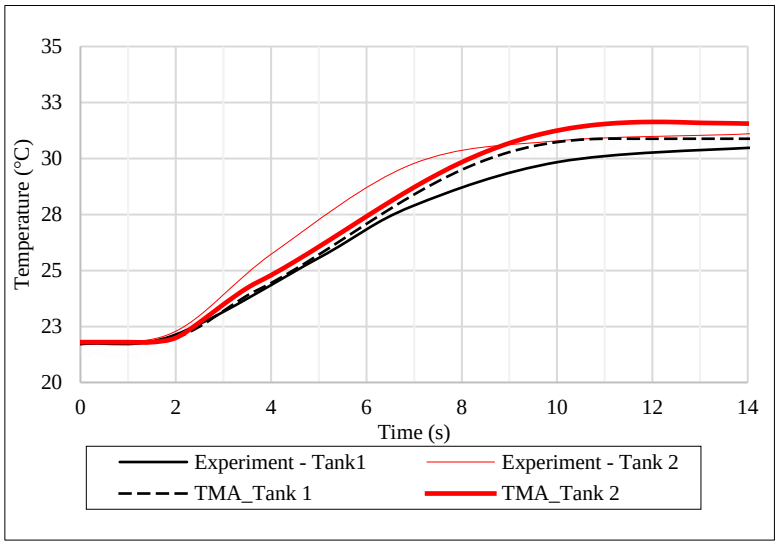

Figure 7. Comparison of rolling average simulated temperature against experimentally measured temperature.

One possible explanation for the unexpected experimental temperature growth in the onboard tanks after hydrogen flow stops is that the experimentalists use a smoothing technique such as a rolling average to eliminate temperature oscillations or for other reasons. This is a common practice among experimentalists [34] as temperature oscillations at the thermocouple location could be imposed by

continuous changes in temperature due to flow turbulence and swirls of the non-uniform temperature inside the tank. In fact, doing a rolling average could also act as a physical rolling average of the experimentally measured temperature by an inertial thermocouple. As triple moving average (TMA) was used in other experimental studies [34], this method is chosen to mimic experimental smoothing for the simulated data. Fig. 7 displays a TMA over 10 last reported values of the simulated temperature in two tanks obtained during simulations (effectively resulting in averaging over 5 last seconds given the data was recorded every 0.5 s). The deviation of the simulated temperature from the experimental temperature in this case is within the accuracy of the thermocouples used in the experiments, which is +1.5 K [19].

5.0 CONCLUSIONS

The originality of this study is the development of a unique computational fluid dynamics (CFD) model that can simulate an entire hydrogen fuelling station, including all its components, such as high-pressure tanks, pipes, pressure control valves, mass flow meter, heat exchanger, breakaway, nozzle, and three onboard tanks. The critical components of the hydrogen fuelling station, namely the pressure control valve (PCV) and the heat exchanger (HE), are modelled using an in-house developed code that can regulate the mass flow rate in the PCV and the temperature in the HE. The CFD model successfully replicates the pressure and temperature data obtained from experiments during the start-up phase of the hydrogen fuelling process in the onboard tanks.

This work is significant because it provides an affordable CFD model that can be used to develop hydrogen fuelling protocols for various applications. The CFD model can simulate the entire 14 seconds of the start-up phase in just 2 hours. Additionally, unlike reduced models, the CFD model can predict temperature non-uniformity in onboard tanks, which is crucial in preventing tank failure, particularly in tanks with high L/D ratios.

The rigour of this model is its validation against unique NREL experimental data for temperature and pressure in the onboard storage tanks during the start-up phase of the refuelling process in an actual hydrogen refuelling station. The validation showed that the CFD model is capable of accurately predicting the pressure and temperature dynamics in the onboard storage tanks during the start-up phase of the refuelling process. This is a significant advancement in the field, as it demonstrates the ability of CFD models to be used for studying the dynamics of hydrogen fuelling in real-life HRSs, which was not previously possible.

ACKNOWLEDGEMENTS

This research has received funding from the Fuel Cells and Hydrogen 2 Joint Undertaking (now Clean Hydrogen Partnership) under the European Union's Horizon 2020 research and innovation programme through the SH2APED project under grant agreement No.101007182. The authors are grateful to the Engineering and Physical Sciences Research Council (EPSRC) of the UK for funding through the EPSRC Centre for Doctoral Training in Sustainable Hydrogen "SusHy" (Grant EP/S023909/1), and performing simulations using the Tier 2 High-Performance Computing resources provided by the Northern Ireland High-Performance Computing (NI-HPC) facility funded by the EPSRC (grant EP/T022175/1, https://www.ni-hpc.ac.uk/Kelvin2/). The authors are thankful to Dr Taichi Kuroki from NREL for providing information regarding the experimental details.

REFERENCES

[1] Fuel Cell Standards Committee. J2579_201806 Standard for Fuel Systems in Fuel Cell and Other Hydrogen Vehicles 2018. https://doi.org/10.4271/J2579_201806.

[2] United Nations Economic Commission for Europe. Global Registry. Addendum 13: Global Technical Regulation No. 13. Global Technical Regulation on Hydrogen and Fuel Cell Vehicles 2013.

[3] United Nations. Uniform provisions concerning the approval of motor vehicles and their components with regard to the safety-related performance of hydrogen-fuelled vehicles (HFCV) UN R134. Ece/Trans/Wp29/2014/78 2015.

[4] De Miguel N, Acosta B, Baraldi D, Melideo R, Ortiz Cebolla R, Moretto P. The role of initial tank temperature on refuelling of on-board hydrogen tanks. Int J Hydrogen Energy 2016;41:8606–15. https://doi.org/10.1016/j.ijhydene.2016.03.158.

[5] Fuel Cell Standards Committee. J2601_202005, Fueling Protocols for Light Duty Gaseous Hydrogen Surface Vehicles, Rev 2020. SAE Int 2020:1–2. https://doi.org/10.4271/J2601_202005.

[6] SAE International. SAE J2601-2 - Fueling Protocol for Gaseous Hydrogen Powered Heavy Duty Vehicles. SAE Int 2014.

[7] SAE International. SAE J2601-3 - Fueling Protocol for Gaseous Hydrogen Powered Industrial Trucks. SAE Int 2022.

[8] ISO/TS 15869 Gaseous hydrogen and hydrogen blends — Land vehicle fuel tanks 2009.

[9] Sun K, Li Z. Development of emergency response strategies for typical accidents of hydrogen fuel cell electric vehicles. Int J Hydrogen Energy 2021;46:37679–96. https://doi.org/10.1016/j.ijhydene.2021.02.130.

[10] Lazarenko O, Parkhomenko V-P, Sukach R, Bilonozhko B, Kuskovets A. Design Features and Hazards of Hydrogen Fuel Cell Cars. Fire Saf 2021;37:52–7. https://doi.org/10.32447/20786662.37.2020.08.

[11] Zheng J, Guo J, Yang J, Zhao Y, Zhao L, Pan X, Ma J, Zhang L. Experimental and numerical study on temperature rise within a 70 MPa type III cylinder during fast refueling. Int J Hydrogen Energy 2013;38:10956–62. https://doi.org/10.1016/j.ijhydene.2013.02.053.

[12] Melideo D, Baraldi D, Galassi MC, Ortiz Cebolla R, Acosta Iborra B, Moretto P. CFD model performance benchmark of fast filling simulations of hydrogen tanks with pre-cooling. Int J Hydrogen Energy 2014;39:4389–95. https://doi.org/10.1016/j.ijhydene.2013.12.196.

[13] Bourgeois T, Brachmann T, Barth F, Ammouri F, Baraldi D, Melideo D, Acosta-Iborra B, Zaepffel D, Saury D, Lemonnier D. Optimization of hydrogen vehicle refuelling requirements. Int J Hydrogen Energy 2017;42:13789–809. https://doi.org/10.1016/j.ijhydene.2017.01.165.

[14] Hosseini M, Dincer I, Naterer GF, Rosen MA. Thermodynamic analysis of filling compressed gaseous hydrogen storage tanks. Int J Hydrogen Energy 2012;37:5063–71. https://doi.org/10.1016/j.ijhydene.2011.12.047.

[15] Molkov V, Dadashzadeh M, Makarov D. Physical model of onboard hydrogen storage tank thermal behaviour during fuelling. Int J Hydrogen Energy 2019;44:4374–84. https://doi.org/10.1016/j.ijhydene.2018.12.115.

[16] Bai Y, Zhang C, Duan H, Jiang S, Zhou Z, Grouset D, Zhang M, Ye X. Modeling and optimal control of fast filling process of hydrogen to fuel cell vehicle. J Energy Storage 2021;35:102306. https://doi.org/10.1016/j.est.2021.102306.

[17] Kuroki T, Sakoda N, Shinzato K, Monde M, Takata Y. Dynamic simulation for optimal hydrogen refueling method to Fuel Cell Vehicle tanks. Int J Hydrogen Energy 2018;43:5714–21. https://doi.org/10.1016/j.ijhydene.2018.01.111.

[18] Charolais A, Ammouri F, Vyazmina E, Nouvelot Q, Guewouo T, Greisel M, Gebhard M, Kuroki T, Mathison S. Protocol for heavy duty hydrogen refueling: a modeling benchmark. Int. Conf. Hydrog. Saf., Edinburgh: 2021, p. 1150–60.

[19] Kuroki T, Nagasawa K, Peters M, Leighton D, Kurtz J, Sakoda N, Monde M, Takata Y. Thermodynamic modeling of hydrogen fueling process from high-pressure storage tank to vehicle tank. Int J Hydrogen Energy 2021;46:22004–17. https://doi.org/10.1016/j.ijhydene.2021.04.037.

[20] Carrere P, Lodiar G, Vyazmina E, Ammouri F, Charolais A. CFD simulations of the refueling of long horizontal H2 tanks. Int. Conf. Hydrog. Saf., Edinburgh: 2021, p. 1175–84.

[21] Melideo D, Baraldi D. CFD analysis of fast filling strategies for hydrogen tanks and their effects on key-parameters. Int J Hydrogen Energy 2015;40:735–45. https://doi.org/10.1016/j.ijhydene.2014.10.138.

[22] Melideo D, Baraldi D, Acosta-Iborra B, Cebolla RO, Moretto P. Cfd Investigation of Filling and Emptying of Hydrogen Tanks. Proc Int Conf Hydrog Saf 2015:1–12.

[23] Melideo D, Baraldi D, Galassi MC, Ortiz Cebolla R, Acosta Iborra B, Moretto P. Assessment of a CFD Model for the Simulation of Fast Filling of Hydrogen Tanks With Pre-Cooling. Int Conf Hydrog Saf n.d.:1–11.

[24] Zheng J, Guo J, Yang J, Zhao Y, Zhao L, Pan X, Ma J, Zhang L. Experimental and numerical study on temperature rise within a 70 MPa type III cylinder during fast refueling. Int J Hydrogen Energy 2013;38:10956–62. https://doi.org/10.1016/j.ijhydene.2013.02.053.

[25] Bourgeois T, Brachmann T, Barth F, Ammouri F, Baraldi D, Melideo D, Acosta-Iborra B, Zaepffel D, Saury D, Lemonnier D. Optimization of hydrogen vehicle refuelling requirements. Int J Hydrogen Energy 2017;42:13789–809. https://doi.org/10.1016/j.ijhydene.2017.01.165.

[26] Heitsch M, Baraldi D, Moretto P. Numerical investigations on the fast filling of hydrogen tanks. Int J Hydrogen Energy 2011;36:2606–12. https://doi.org/10.1016/j.ijhydene.2010.04.134.

[27] Ramasamy V, Richardson ES. Thermal response of high-aspect-ratio hydrogen cylinders undergoing fast-filling. Int J Heat Mass Transf 2020;160:120179. https://doi.org/10.1016/j.ijheatmasstransfer.2020.120179.

[28] Bourgeois T, Ammouri F, Baraldi D, Moretto P. The temperature evolution in compressed gas filling processes: A review. Int J Hydrogen Energy 2018;43:2268–92. https://doi.org/10.1016/j.ijhydene.2017.11.068.

[29] Miller R. Flow measurement engineering handbook. 3rd ed. McGraw-Hill; 1983.

[30] Lemmon EW, Bell IH, Huber ML, McLinden MO. NIST Standard Reference Database 23: Reference Fluid Thermodynamic and Transport Properties-REFPROP, Version 10.0, National Institute of Standards and Technology, Standard Reference Data Program, Gaithersburg, 2018 n.d. https://doi.org/10.18434/T4/1502528.

[31] Launder BE, Spalding DB. The numerical computation of turbulent flows. Comput Methods Appl Mech Eng 1974;3:269–89. https://doi.org/10.1016/0045-7825(74)90029-2.

[32] Ansys Inc. Ansys® Fluent 2020 R2 User Manual 2020. https://ansyshelp.ansys.com/account/secured?returnurl=/Views/Secured/corp/v202/en/ (accessed October 4, 2022).

[33] Simonovski I, Baraldi D, Melideo D, Acosta-Iborra B. Thermal simulations of a hydrogen storage tank during fast filling. Int J Hydrogen Energy 2015;40:12560–71. https://doi.org/10.1016/j.ijhydene.2015.06.114.

[34] Hart N, Sinding CD, Mathison S, Quong S, Mattelaer V, Ruiz A, Grab A, Kvasnicka A, Spitta C, Ammouri F, Vyazmina E, Ren V, et al. PRHYDE Results as Input for Standardisation. Deliverable D6.7. 2022.